

**Interplay of covalency, spin-orbit coupling, and geometric frustration in the  $d^{3.5}$  system  $\text{Ba}_3\text{LiIr}_2\text{O}_9$** 

Jayita Chakraborty\*

*Department of Physics, Indian Institute of Science Education and Research Bhopal, Bhauri, Bhopal 462066, India*

(Received 21 February 2018; revised manuscript received 14 May 2018; published 27 June 2018; corrected 19 August 2019)

The electronic and magnetic properties of  $d^{3.5}$  iridate  $\text{Ba}_3\text{LiIr}_2\text{O}_9$  have been studied using first-principles electronic structure calculations. The results of the calculations reveal that the system lies in an intermediate spin-orbit coupling (SOC) regime. There is strong covalency of Ir-5*d* and O-2*p* orbitals. SOC, together with covalency, conspires to reduce the magnetic moment at the Ir site. By calculating the hopping interactions and exchange interactions, it is found that there is strong antiferromagnetic intradimer coupling within an  $\text{Ir}_2\text{O}_9$  unit and other antiferromagnetic interdimer interactions make the system frustrated. The anisotropic magnetic interactions are also calculated. The calculations reveal that the magnitude of the Dzyaloshinskii-Moriya interactions parameter is small for this system. The magnetocrystalline anisotropy energy is large for this system and the easy axis lies on the *ab* plane.

DOI: [10.1103/PhysRevB.97.235147](https://doi.org/10.1103/PhysRevB.97.235147)**I. INTRODUCTION**

The interplay of strong spin-orbit coupling, electron-electron correlation, and crystal-field splitting have recently attracted much attention both theoretically and experimentally [1,2]. Iridium oxides offer an excellent playground for such an interplay and exhibit intriguing phenomena. Many exotic phases like novel Mott insulating states, spin-liquid states, orbital oriented exchange coupling in Kitaev-type models, topological Mott insulators, Weyl semimetals, and topological magnetic insulators with axionic excitations have been found in these materials [3–6]. As a result, both experimental and theoretical efforts have been undertaken to investigate novel spin-orbit physics in various 5*d* systems. Iridates with 4+ ( $5d^5$ ) and 5+ ( $5d^4$ ) oxidation state of Ir have been much explored and found to exhibit interesting phenomena [7–10]. Realization of  $J_{\text{eff}} = 1/2$  and  $J_{\text{eff}} = 0$  states are observed with  $d^5$  and  $d^4$  valence states of Ir respectively [3,11]. However, iridates with the higher oxidation state of Ir are hardly studied. The hexavalent systems (6+ oxidation state,  $d^3$  configuration) are generally assumed to possess spin-only  $S = \frac{3}{2}$  ground states with quenched orbital angular momentum according to the usual *L-S* coupling scheme. This scenario is however not true in the presence of strong spin-orbit coupling (SOC). Interesting spin-orbit driven magnetism is found in  $4d^3$  and  $5d^3$  based transition-metal oxides [12–14].

The 6*H* triple perovskite iridates with the general formula  $\text{Ba}_3\text{M}\text{Ir}_2\text{O}_9$  attracted much attention because the valency of Ir can be tailored by nonmagnetic *M* atom [11,15,16]. The spin-orbital liquid state is found for  $\text{Ba}_3\text{ZnIr}_2\text{O}_9$  [11]. The fractional valence state of Ir ( $d^{4.5}$ ) is also found in these triple perovskite systems. Spin-orbit driven magnetism is found for  $\text{Ba}_3\text{YIr}_2\text{O}_9$  and  $\text{Ba}_3\text{InIr}_2\text{O}_9$  [15,16]. Another 6*H*-triple perovskite  $\text{Ba}_3\text{LiIr}_2\text{O}_9$  is synthesized by Kim *et al.*, where Ir is in a fractional oxidation state of +5.5 [17]. The magnetic

moments determined from the temperature dependence of the magnetic susceptibility are low for this compound and the value of magnetic moment at an Ir site is much smaller than the spin only value. The spin-orbit coupling may play an important role in this system. It is expected that the iridates with the higher oxidation state of Ir have strong covalency with Ir-5*d* and O-2*p* states. Zero-field-cooled (ZFC) and field cooled (FC) data for magnetic susceptibility diverge at 75 K, suggesting the presence of the frustration in this system [17]. The combined effect of strong covalency, geometric frustration, and spin-orbit coupling may lead to intriguing phases in this material. In spite of all the work that has been done on  $5-d^4$ ,  $5-d^{4.5}$ , and  $5-d^5$  iridates, there has been very little progress in iridates containing Ir with higher oxidation states. In  $\text{Ba}_3\text{LiIr}_2\text{O}_9$ , Ir is in the fractional oxidation state of 5.5 (i.e.,  $5-d^{3.5}$  state). In this context, first-principles electronic structure calculations based on density functional theory (DFT) are important for investigating the effect of covalency, geometric frustration, and spin-orbit coupling in this material.

In this paper, the electronic and magnetic properties of  $\text{Ba}_3\text{LiIr}_2\text{O}_9$  are studied using first-principles calculations within the framework of density functional theory. The aim of this study is to understand the cross coupling between spin, geometric frustration, covalency, and spin-orbit interaction in this  $d^{3.5}$  iridate. The nature of magnetism in  $\text{Ba}_3\text{LiIr}_2\text{O}_9$  is studied by determining the magnitude of the relevant magnetic interactions including the isotropic exchange, the Dzyaloshinskii-Moriya (DM) coupling, and the magnetocrystalline anisotropy, by projecting the total energies for different magnetically constrained spin configurations onto a spin Hamiltonian. The possible spin model of  $\text{Ba}_3\text{LiIr}_2\text{O}_9$  is proposed here.

**II. CRYSTAL STRUCTURE AND METHOD**

$\text{Ba}_3\text{LiIr}_2\text{O}_9$  crystallizes in a 6*H*-perovskite-type structure with space group *P63/mmc*. The unit cell, as depicted in Fig. 1, contains two formula units. Ir is in the octahedral environment with oxygen atoms. Each distorted  $\text{IrO}_6$  octahedron shares

\*jayita@iiserb.ac.in

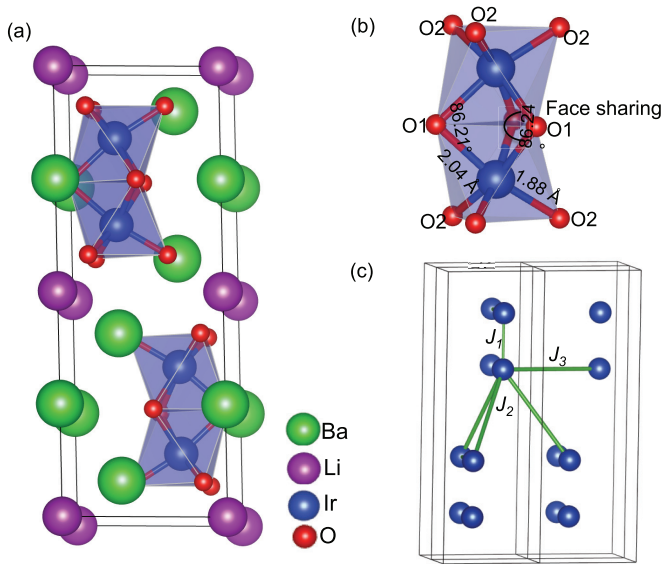


FIG. 1. (a) The unit cell of  $\text{Ba}_3\text{LiIr}_2\text{O}_9$  (viewed from  $b$  axis), (b)  $\text{Ir}_2\text{O}_9$  face-shared bioctahedra. (c) The exchange interaction paths are indicated here.

a face with the neighboring one, forming  $\text{Ir}_2\text{O}_9$  face-shared bioctahedra. There are two structural Ir dimers in the unit cell which are connected via O-Li-O paths along the  $c$  axis.

To study the electronic structure and magnetic properties of  $\text{Ba}_3\text{LiIr}_2\text{O}_9$ , the first-principles electronic structure calculations have been performed within the framework of density functional theory. Two different methods are used in this work: (i) the plane-wave based projector augmented wave (PAW) [18] method as implemented in the VASP code [19], and (ii) muffin-tin based linearized muffin-tin orbital (LMTO) method within atomic sphere approximation (ASA) [20] and  $N$ th-order muffin-tin orbital (NMTO) downfolding method [21]. The NMTO downfolding method is used to get a few band low-energy Hamiltonian. The self-consistent potentials from LMTO calculations are used in NMTO calculations. No empty sphere was used for the LMTO calculations within the atomic sphere approximation (ASA). The space filling MT radii used for Ba, Li, Ir, and O are 2.24, 1.47, 1.30, and 0.97 Å, respectively.

The kinetic energy cutoff of 500 eV was used for plane-wave calculations.  $11 \times 11 \times 5$   $k$  points following the Monkhorst-Pack scheme has been used for the Brillouin-zone integration for this compound. Local-density approximation (LDA) is used for the exchange correlation functional. To properly describe the electron correlation associated with the  $5d$  states of Ir, the LDA+ $U$  method is used in the calculations [22]. The convergence threshold for the electronic structure is  $10^{-5}$  eV for without spin-orbit coupling (SOC) and  $10^{-7}$  eV for the calculations with SOC. The atomic positions are optimized with the lattice parameters fixed at the experimental values. For the crystal orbital Hamiltonian population (COHP) calculations the LOBSTER code is used [23]. Here COHP is constructed from plane-wave based self-consistent calculations.

The anisotropic magnetic interactions are calculated from the *ab initio* method. Here the Dzyaloshinskii-Moriya (DM) [24,25] coupling parameters are calculated by compar-

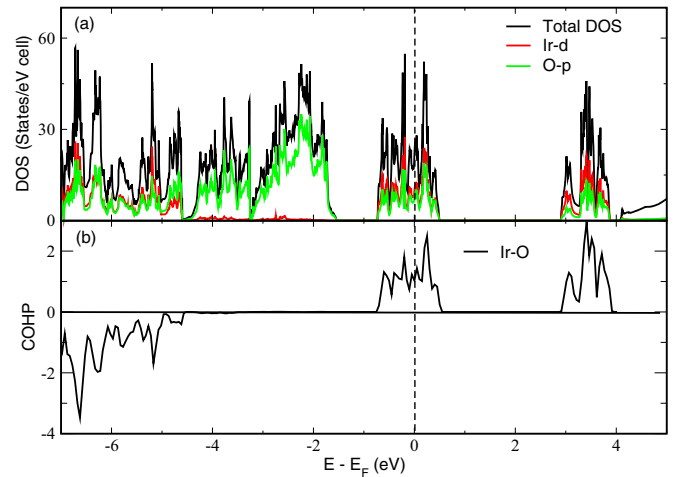


FIG. 2. (a) The spin unpolarized total and orbital projected density of states, (b) COHP for Ir-O bond within an octahedron of  $\text{Ba}_3\text{LiIr}_2\text{O}_9$ .

ing the total energy of selected noncollinear spin configurations [26]. The total energy of noncollinear spin configurations is calculated by constraining the magnetic moment along specific directions [27]. A penalty contribution to the total energy is considered in these calculations. The penalty energy fixes the local moment into a specific direction,

$$E = E_0 + \sum_i \gamma [\vec{M}_i - \hat{M}_i^0 (\hat{M}_i^0 \cdot \vec{M}_i)]^2, \quad (1)$$

where  $E_0$  is the DFT energy without any constraint and the second term represents the penalty energy contribution due to the noncollinear directional constraint.  $\hat{M}_i^0$  is a unit vector along the desired direction of the magnetic moment at site  $i$  and  $\vec{M}_i$  is the integrated magnetic moment inside the Wigner-Seitz cell around the atom  $i$ . The parameter  $\gamma$  controls the penalty energy contribution [28]. In these calculations, the penalty energy reduces to  $< 10^{-5}$  eV for  $\gamma = 10$ .

### III. ELECTRONIC STRUCTURE

To start with, the electronic structure of  $\text{Ba}_3\text{LiIr}_2\text{O}_9$  has been analyzed without any magnetic order. Figure 2(a) displays the spin unpolarized total and orbital projected density of states (DOS) for this system. The Ba- $6s$  and Li- $2s$  states are empty and hence lie far above the Fermi energy ( $E_F$ ). O- $2p$  states are mostly occupied though they hybridize strongly with the Ir- $5d$  states indicating strong covalency of the Ir-O bond. Due to the octahedral environment, the Ir- $5d$  states are split into  $t_{2g}$  and  $e_g$  [see Fig. 2(a)]. The DOS is consistent with the nominal ionic formula  $\text{Ba}_3^{2+}\text{Li}^+\text{Ir}_2^{5.5+}\text{O}_9^{2-}$  for the system.

Further, an energy-resolved visualization of the chemical bonding between Ir and O atoms within an octahedron is obtained from the crystal orbital Hamiltonian population (COHP) plot as shown in Fig. 2(b). In COHP, the DOS is weighted by the Hamiltonian matrix elements where the off-site COHP represents the covalent contribution to bands. The bonding contribution for which the system undergoes a lowering of energy is indicated by negative COHP and the antibonding contribution that raises the energy is represented by positive

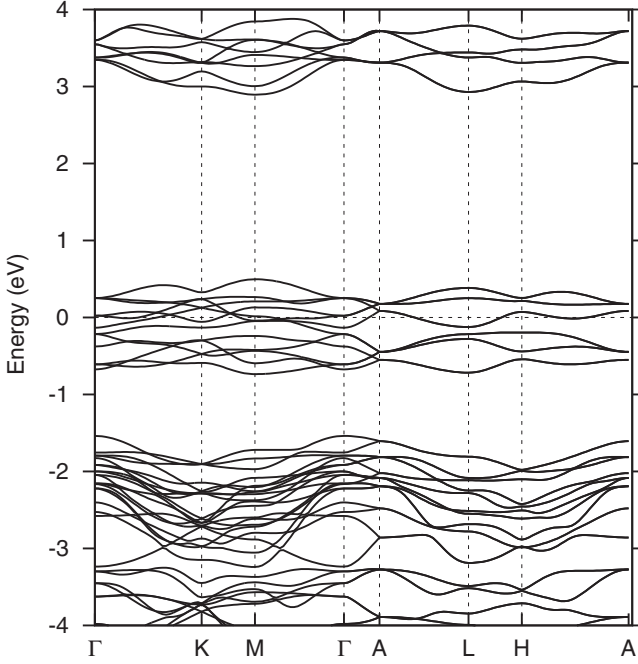


FIG. 3. The band structure of  $\text{Ba}_3\text{LiIr}_2\text{O}_9$  within LDA.

COHP. Thus it gives a quantitative measure of bonding. In Fig. 2(b), the off-site COHP is plotted. The calculation of COHP reveals that the Ir-O covalency is substantially strong in this system. As expected, the value of COHP near the Fermi level is less compared to the value of COHP for  $d^3$  iridates  $\text{Sr}_2\text{MIrO}_6$  ( $M = \text{Mg}, \text{Ca}$ ) [14]. Due to the higher oxidation state of Ir ( $\text{Ir}^{6+}$ ) in  $\text{Sr}_2\text{MIrO}_6$ , the chemical bonding between Ir(6+) and O is stronger compared to the  $\text{Ba}_3\text{LiIr}_2\text{O}_9$  ( $d^{3.5}$  iridates).

The spin unpolarized band structure is shown in Fig. 3. The characteristic feature of the band structure is the isolated manifold of 12  $t_{2g}$  bands hosting the Fermi level ( $E_F$ ) arising from the four Ir atoms in the unit cell. These 12  $t_{2g}$  bands are well separated from eight  $e_g$  bands.

#### Crystal-field splitting and hopping interactions

In order to find the crystal-field splitting of Ir- $d$  orbitals in the distorted octahedral environment and hopping interactions between various Ir atoms, the NMTO downfolding method is employed. To calculate crystal-field splitting, only Ir- $5d$  orbitals are retained in the basis and the rest are downfolded. The diagonalization of the on-site block of  $5 \times 5$  Hamiltonian gives the crystal-field splitting for Ir- $5d$  states including the covalency with oxygens. These energies are calculated to be  $-4.4045, -4.4045, -4.3767, -0.8383$ , and  $-0.8383$  eV. The corresponding eigenstates are

$$\begin{aligned}
 |1\rangle &= -0.81|xy\rangle + 0.59|yz\rangle, \\
 |2\rangle &= 0.59|xz\rangle + 0.81|x^2 - y^2\rangle, \\
 |3\rangle &= |3z^2 - r^2\rangle, \\
 |4\rangle &= -0.81|xz\rangle + 0.59|x^2 - y^2\rangle, \\
 |5\rangle &= -0.59|xy\rangle - 0.81|yz\rangle.
 \end{aligned} \tag{2}$$

TABLE I. The hopping parameters (in meV) obtained from NMTO downfolding method for  $\text{Ba}_3\text{LiIr}_2\text{O}_9$  are listed here. The interaction paths ( $t_1$ ,  $t_2$ , and  $t_3$ ) are indicated in Fig. 1(c).

Hopping parameter	Distance ( $\text{\AA}$ )	Orbital involved			
			1)	2)	3)
$t_1$	2.76	(1)	-139.2	258.5	0
		(2)	-258.5	-290.4	0
		(3)	0	0	-40.4
$t_2$	5.52	(1)	112	23	123
		(2)	23	16.5	10.9
		(3)	123	10.9	-71
$t_3$	5.78	(1)	20.3	42.1	12
		(2)	23	-52.1	42.3
		(3)	14.9	-41.1	-20.9

It is clear that |1) and |2) are degenerate and slightly separated from |3). These form a  $t_{2g}$  manifold. Due to trigonal distortion of the octahedron, the manifold splits into low-lying doubly degenerate states |1) and |2) known as  $e_g^T$  states and a singlet state |3) known as a  $a_1$  state [29]. The original  $e_g$  doublet remains unsplit. The  $t_{2g}$ - $e_g$  crystal-field splitting is quite large ( $\sim 3.5$  eV) which is also visible in the plot of the partial DOS in Fig. 2. In the strong octahedral field, the Ir having a nominal oxidation state  $3.5+$  will exhibit a low spin configuration ( $t_{2g}^{3.5}, e_g^0$ ) and hence  $t_{2g}$  orbitals are the active orbitals of this system. For calculations of hopping interactions, only  $t_{2g}$  orbitals are retained in the basis and the rest are downfolded. The hopping interactions are listed in Table I. Due to the very small distance between Ir atoms within the  $\text{Ir}_2\text{O}_9$  unit, strong direct hopping  $t_1$  is found for the system. The next-nearest-neighbor (NNN) hopping  $t_2$  is also substantial. It is supersuperexchange interaction via the exchange path Ir-O-Li-O-Ir.

#### IV. MAGNETISM AND EFFECT OF SPIN-ORBIT COUPLING

To investigate the magnetic properties of this system, four different magnetic configurations are simulated. These configurations are (i) FM [both nearest-neighbor (NN) and next-nearest-neighbor (NNN) couplings are ferromagnetic], (ii) AF1 (both the NN and NNN couplings are antiferromagnetic), AF2 (NN coupling is ferromagnetic and NNN coupling is antiferromagnetic), and finally AF3 (NN coupling is antiferromagnetic and NNN coupling is ferromagnetic) (see Fig. 1 of the Supplemental Material [30]). The calculations reveal that AF1 is lowest in energy within LSDA+ $U$  for  $U = 1.5$  and 3 eV (see Table 1 of the Supplemental Material [30]). Interestingly, the moment at the Ir site reduces appreciably for all the configurations and the oxygen atoms acquire substantial moment due to strong hybridization of Ir- $5d$  and O- $2p$  states.

To find the importance of spin-orbit coupling in  $\text{Ba}_3\text{LiIr}_2\text{O}_9$ , the total-energy calculations have been done for four different magnetic configurations, namely FM, AF1, AF2, and AF3 with spin-orbit coupling. A small but finite orbital moment  $0.03$ – $0.15\mu_B$  at the Ir site appears within LSDA+ $U$ +SOC calculations. Figure 4 reveals that the magnitude of spin and

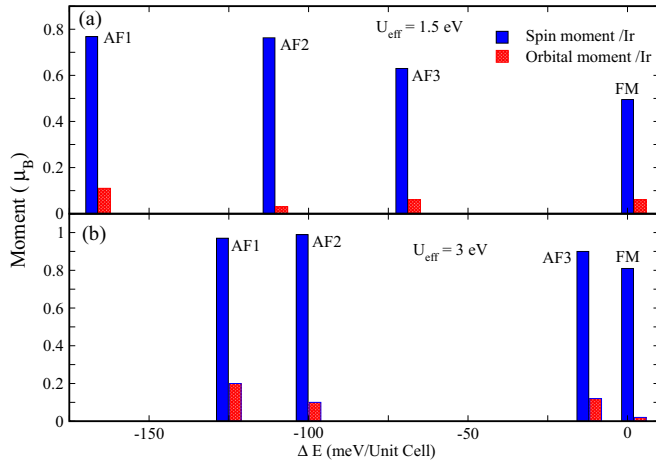


FIG. 4. The variation of spin and orbital moment at the Ir site for various magnetic configurations within LDA+ $U$ +SOC for (a)  $U_{\text{eff}} = 1.5$  eV and (b)  $U_{\text{eff}} = 3$  eV are graphically represented here.

orbital moments at the Ir site fluctuate for different magnetic configurations. Among the various magnetic configurations, AF1 is lowest in energy and the system is insulating only for the AF1 configuration as illustrated by the plot of density of states shown in Fig. 5.

To find out different magnetic interactions in this system, the following spin Hamiltonian is considered:

$$H = - \underbrace{\sum_{i,j} J_{ij} \vec{S}_i \cdot \vec{S}_j}_{\text{symmetric}} + \underbrace{\sum_{\langle ij \rangle} \vec{D}_{ij} \cdot (\vec{S}_i \times \vec{S}_j)}_{\text{antisymmetric}} + \underbrace{\sum_i \epsilon_{an}^i |\vec{S}_i|^2}_{\text{anisotropy}}, \quad (3)$$

where the first, second, and last terms represent the isotropic exchange, the antisymmetric part of the exchange interaction (also called the Dzyaloshinskii-Moriya interaction), and the single-site anisotropy (SSA) respectively. Here,  $\vec{S}_i$  is on the Ir site. Determining the exchange interaction from fitting the total energy of different spin configurations works reasonably well for localized  $t_{2g}$  states of the Ir in many irridates [11,14,28].

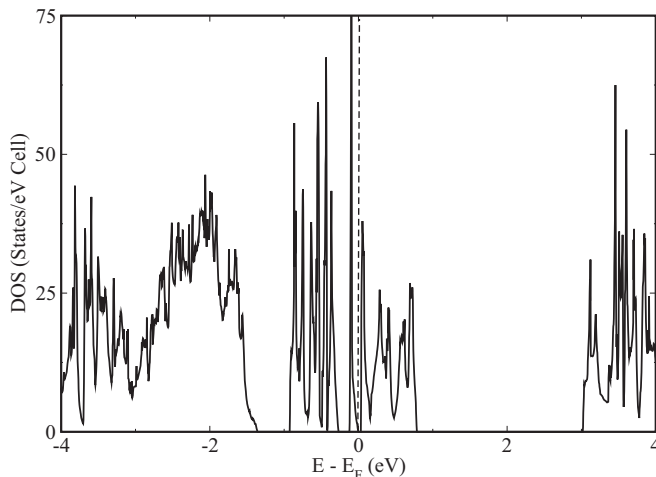


FIG. 5. Total density of states for AF1 configuration within LDA+ $U$ +SOC for  $U_{\text{eff}} = 1.5$  eV.

### A. Symmetric exchange interactions

The symmetric exchange interactions are calculated from different collinear magnetic configurations (FM, AF1, AF2, and AF3) to provide insight into the geometrical frustration in  $\text{Ba}_3\text{LiIr}_2\text{O}_9$ . The exchange interactions are calculated up to third-nearest neighbor by mapping the total energies of four magnetic configurations obtained within LSDA+ $U$  calculation into the spin Hamiltonian [see Eq. (3)]. Here,  $J_{ij} < 0$  implies an antiferromagnetic while  $J_{ij} > 0$  indicates a ferromagnetic-type exchange interaction. Two different values of  $U$  (1.5 and 3 eV) have been used in these calculations. The values of exchange interactions  $J_1$ ,  $J_2$ , and  $J_3$  are  $-3.43$ ,  $-2.80$ , and  $1.69$  meV for  $U_{\text{eff}} = 1.5$  eV and  $-2.26$ ,  $-1.53$ , and  $0.63$  meV for  $U_{\text{eff}} = 3.0$  eV respectively. The exchange paths  $J_1$ ,  $J_2$ , and  $J_3$  are indicated in Fig. 1(c). The strongest interaction is intradimer exchange interaction  $J_1$  and it is an antiferromagnetic type. The second large exchange interaction is  $J_2$  which is also an antiferromagnetic type. These two antiferromagnetic-type interactions make the system frustrated. The third-nearest-neighbor interaction  $J_3$  is a ferromagnetic type. As expected, antiferromagnetic  $J_1$  and  $J_2$  decrease with increasing  $U$  values [31].

### B. Antisymmetric exchange interactions

Next, the antisymmetric part of the spin Hamiltonian [second part of Eq. (3)] is considered and the Dzyaloshinskii-Moriya interaction parameters ( $\vec{D}$ ) are calculated from the total-energy calculations within LSDA+ $U$ +SOC for  $U_{\text{eff}} = 1.5$  eV [26]. The three components  $D_{12}^x$ ,  $D_{12}^y$ ,  $D_{12}^z$  of the DM vector (between nearest-neighbor spin sites 1 and 2) are calculated for this system. In order to calculate the  $x$  component of  $\vec{D}_{12}$ , the following four spin configurations are considered in which the spins 1 and 2 are oriented along the  $y$  and  $z$  axes, respectively: (i)  $S_1 = (0, S, 0)$ ,  $S_2 = (0, 0, S)$ , (ii)  $S_1 = (0, -S, 0)$ ,  $S_2 = (0, 0, S)$ , (iii)  $S_1 = (0, S, 0)$ ,  $S_2 = (0, 0, -S)$ , (iv)  $S_1 = (0, -S, 0)$ ,  $S_2 = (0, 0, -S)$ . In these four spin configurations, the spins of all the other spin sites are the same and are along the  $x$  direction. The spin interaction energy for the four spin configurations can be written as

$$E_{\text{spin}} = E_o + D_{12}^x S_1^y S_2^z - S_1^y \sum_{i=3,4} D_{1i}^z S_i^x + S_2^z \sum_{i=3,4} D_{2i}^y S_i^x,$$

and similarly for  $y$  and  $z$  components of  $\vec{D}_{12}$ . The calculated values (in meV) for  $U_{\text{eff}} = 1.5$  eV are  $D_{12}^x S^2 = -0.54 \times 10^{-4}$ ,  $D_{12}^y S^2 = 0.06$ , and  $D_{12}^z S^2 = 0.007$  and the magnitude of the DM vector is  $0.64 \times 10^{-2}$  meV ( $\frac{|D_{12}|}{J_1} = 0.01$ ). The DM interaction, which prefers an orthogonal coupling of the spins, is much weaker than the isotropic exchange interaction in this system. Although the magnitude of DM vector is small compared to other  $d^4$  irridates [28], nevertheless these calculations suggest that SOC has a profound impact on magnetism in the  $d^{3.5}$  irridate  $\text{Ba}_3\text{LiIr}_2\text{O}_9$ .

The effect of electron and hole doping in quasi-two-dimensional irridates gives rise to interesting physics [32–34]. The recent experiment shows the Fermi arcs and the pseudogap physics in the electron and hole-doped irridates [35–37]. The DM interactions can also change with the small electron and/or hole doping in the irridates [38]. In order to investigate that

TABLE II. The energy difference/Ir within LDA+ $U$ +SOC calculations with different spin quantization axis are listed here.

Spin quantization axis	$U_{\text{eff}} = 1.5$ eV $\Delta E$ (meV)	$U_{\text{eff}} = 3$ eV $\Delta E$ (meV)
(001)	0	0
(010)	-4.17	-11.03
(100)	-4.19	-11.18

the effect of electron and hole doping on DM interactions in  $\text{Ba}_3\text{LiIr}_2\text{O}_9$ , the calculations are done with 6.25% electron and hole doping. The calculated values (in meV) for 6.25% electron doping for  $U_{\text{eff}} = 1.5$  eV are  $D_{12}^y S^2 = -0.34 \times 10^{-4}$ ,  $D_{12}^x S^2 = .016$  and  $D_{12}^z S^2 = 0.003$  meV. For 6.25% hole doping case, the DM parameters are  $D_{12}^x S^2 = -0.13 \times 10^{-4}$ ,  $D_{12}^y S^2 = .08$  and  $D_{12}^z S^2 = 0.008$  meV. There is no significant change of the values of DM interactions within 6.25% electron or hole doping.

Next, the effect of the breaking of inversion symmetry on nearest-neighbor DM interaction is also studied here. The distortion in  $\text{IrO}_6$  octahedron [see Fig. 1(b)] of  $\text{Ba}_3\text{LiIr}_2\text{O}_9$ , introduces different Ir-O-Ir angles, which break the local inversion symmetry and give rise to a small value of nearest-neighbor DM interaction. It is very similar to  $\text{Ba}_3\text{CaIr}_2\text{O}_9$  and  $\text{Ba}_3\text{SrIr}_2\text{O}_9$  [10]. If we break the inversion symmetry of the crystal, the Ir-O-Ir angles are much more different from each other ( $84.3^\circ$  and  $85.1^\circ$ ). The values of DM parameters are  $D_{12}^x S^2 = 0.16$ ,  $D_{12}^y S^2 = 0.23$  and  $D_{12}^z S^2 = 0.96$  meV. The values of nearest-neighbor DM interaction parameters are increased in this structure.

### C. Magnetocrystalline anisotropy

Further, the magnetocrystalline anisotropy is calculated by calculating the total energies with different spin quantization

axes [39]. The results of the calculations are listed in Table II. A large value of magnetocrystalline anisotropy is found for this system. The value of the small orbital moment, the small DM vector, and the large magnetocrystalline anisotropy energy suggest that the compound lies in an intermediate regime between the  $LS$  and  $jj$  coupling scheme.

## V. SUMMARY

The electronic and magnetic properties of hexagonal triple perovskite  $\text{Ba}_3\text{LiIr}_2\text{O}_9$  have been studied using first-principles electronic structure calculations within the framework of density functional theory. The crystal-field effect, covalency of Ir-5d and O-2p orbitals, exchange interactions, and importance of spin-orbit coupling in this compound are investigated. There is strong covalency of Ir-5d states with O-2p states as evidenced by partial DOS and the COHP plot. The magnetic moment at the Ir site is substantially reduced from the spin only value upon the inclusion of SOC. The calculated exchange interactions show the presence of geometrical frustration, in agreement with the experimental observation. A small but significant orbital moment has been found at the Ir site, suggesting that SOC together with covalency conspires to reduce the moment at the Ir site. Calculations of the isotropic, single-site anisotropy and Dzyaloshinskii-Moriya (DM) coupling parameters, nearest-neighbor DM interaction parameters, magnetocrystalline anisotropy, and the orbital moment at the Ir site within LSDA+ $U$ +SOC suggest that this system belongs to the intermediate spin-orbit coupling regime.

## ACKNOWLEDGMENTS

I thank Dr. N. Ganguli for fruitful scientific discussions. Use of the high-performance computing facility of IISER Bhopal is gratefully acknowledged.

- 
- [1] W. Witczak-Krempa, G. Chen, Y. B. Kim, and L. Balents, *Annu. Rev. Condens. Matter Phys.* **5**, 57 (2014).
- [2] J. G. Rau, E. K.-H. Lee, and H.-Y. Kee, *Annu. Rev. Condens. Matter Phys.* **7**, 195 (2016).
- [3] B. J. Kim, H. Ohsumi, T. Komesu, S. Sakai, T. Morita, T. Takagi, and H. Arima, *Science* **323**, 1329 (2009).
- [4] B. J. Kim, H. Jin, S. J. Moon, J. Y. Kim, B. G. Park, C. S. Leem, J. Yu, T. W. Noh, C. Kim, S. J. Oh, J. H. Park, V. Durairaj, G. Cao, and E. Rotenberg, *Phys. Rev. Lett.* **101**, 076402 (2008).
- [5] G. Jackeli and G. Khaliullin, *Phys. Rev. Lett.* **102**, 017205 (2009).
- [6] J. J. Kim, A. H. Said, D. Casa, M. H. Upton, T. Gog, M. Daghofer, G. Jackeli, J. van den Brink, G. Khaliullin, and B. J. Kim, *Phys. Rev. Lett.* **109**, 157402 (2012).
- [7] G. Cao, T. F. Qi, L. Li, J. Terzic, S. J. Yuan, L. E. DeLong, G. Murthy, and R. K. Kaul, *Phys. Rev. Lett.* **112**, 056402 (2014).
- [8] O. N. Meetei, W. S. Cole, M. Randeria, and N. Trivedi, *Phys. Rev. B* **91**, 054412 (2015).
- [9] T. Dey, A. Maljuk, D. V. Efremov, O. Kataeva, S. Gass, C. G. F. Blum, F. Steckel, D. Gruner, T. Ritschel, A. U. B. Wolter, J. Geck, C. Hess, K. Koepnick, J. van den Brink, S. Wurmehl, and B. Büchner, *Phys. Rev. B* **93**, 014434 (2016).
- [10] A. Nag, S. Bhowal, F. Bert, A. D. Hillier, M. Itoh, I. Carlomagno, C. Meneghini, T. Sarkar, R. Mathieu, I. Dasgupta, and S. Ray, *Phys. Rev. B* **97**, 064408 (2018).
- [11] A. Nag, S. Middey, S. Bhowal, S. K. Panda, R. Mathieu, J. C. Orain, F. Bert, P. Mendels, P. G. Freeman, M. Mansson, H. M. Ronnow, M. Telling, P. K. Biswas, D. Sheptyakov, S. D. Kaushik, V. Siruguri, C. Meneghini, D. D. Sarma, I. Dasgupta, and S. Ray, *Phys. Rev. Lett.* **116**, 097205 (2016).
- [12] A. A. Aczel, P. J. Baker, D. E. Bugaris, J. Yeon, H.-C. zur Loye, T. Guidi, and D. T. Adroja, *Phys. Rev. Lett.* **112**, 117603 (2014).
- [13] H. Matsuura and K. Miyake, *J. Phys. Soc. Jpn.* **82**, 073703 (2013).
- [14] S. Bhowal and I. Dasgupta, *Phys. Rev. B* **97**, 024406 (2018).
- [15] S. K. Panda, S. Bhowal, Y. Li, S. Ganguly, R. Valentí, L. Nordström, and I. Dasgupta, *Phys. Rev. B* **92**, 180403 (2015).

- [16] T. Dey, M. Majumder, J. C. Orain, A. Senyshyn, M. Prinz-Zwick, S. Bachus, Y. Tokiwa, F. Bert, P. Khuntia, N. Büttgen, A. A. Tsirlin, and P. Gegenwart, *Phys. Rev. B* **96**, 174411 (2017).
- [17] S.-J. Kim, M. D. Smith, J. Darriet, and H.-C. zur Loye, *J. Solid State Chem.* **177**, 1493 (2004).
- [18] P. E. Blöchl, *Phys. Rev. B* **50**, 17953 (1994).
- [19] G. Kresse and J. Furthmüller, *Phys. Rev. B* **54**, 11169 (1996); G. Kresse and D. Joubert, *ibid.* **59**, 1758 (1999).
- [20] O. K. Andersen and O. Jepsen, *Phys. Rev. Lett.* **53**, 2571 (1984); O. K. Andersen, *Phys. Rev. B* **12**, 3060 (1975).
- [21] O. K. Andersen and T. Saha-Dasgupta, *Phys. Rev. B* **62**, R16219 (2000); O. K. Andersen, T. Saha-Dasgupta, and S. Ezhov, *Bull. Mater. Sci.* **26**, 19 (2003).
- [22] S. L. Dudarev, G. A. Botton, S. Y. Savrasov, C. J. Humphreys, and A. P. Sutton, *Phys. Rev. B* **57**, 1505 (1998).
- [23] R. Dronskowski and P. E. Blöchl, *J. Phys. Chem.* **97**, 8617 (1993); V. L. Deringer, A. L. Tchougreff, and R. Dronskowski, *J. Phys. Chem. A* **115**, 5461 (2011); S. Maintz, V. L. Deringer, A. L. Tchougreff, and R. Dronskowski, *J. Comput. Chem.* **34**, 2557 (2013); **37**, 1030 (2016).
- [24] I. Dzyaloshinsky, *J. Phys. Chem. Solids* **4**, 241 (1958).
- [25] T. Moriya, *Phys. Rev.* **120**, 91 (1960).
- [26] H. J. Xiang, E. J. Kan, S.-H. Wei, M.-H. Whangbo, and X. G. Gong, *Phys. Rev. B* **84**, 224429 (2011).
- [27] P. Liu, S. Khmelevskiy, B. Kim, M. Marsman, D. Li, X.-q. Chen, D. D. Sarma, G. Kresse, and C. Franchini, *Phys. Rev. B* **92**, 054428 (2015).
- [28] P. W. Ma and S. L. Dudarev, *Phys. Rev. B* **91**, 054420 (2015).
- [29] D. I. Khomskii, K. I. Kugel, A. O. Sboychakov, and S. V. Streltsov, *J. Exp. Theor. Phys.* **122**, 484 (2016).
- [30] See Supplemental Material at <http://link.aps.org/supplemental/10.1103/PhysRevB.97.235147> for the figure depicting different magnetic configurations (FM, AF1, AF2, AF3) and the table illustrating the energetics of the same.
- [31] J. Chakraborty and I. Dasgupta, *Phys. Rev. B* **86**, 054434 (2012); J. Chakraborty, N. Ganguli, T. Saha-Dasgupta, and I. Dasgupta, *ibid.* **88**, 094409 (2013); B. Koteswararao, A. V. Mahajan, F. Bert, P. Mendels, J. Chakraborty, V. Singh, I. Dasgupta, S. Rayaprol, V. Siruguri, A. Hoser, and S. D. Kaushik, *J. Phys.: Condens. Matter* **24**, 236001 (2012).
- [32] S. Manni, S. Choi, I. I. Mazin, R. Coldea, M. Altmeyer, H. O. Jeschke, R. Valentí, and P. Gegenwart, *Phys. Rev. B* **89**, 245113 (2014).
- [33] E. M. Pärtschke, K. Wohlfeld, K. Foyevtsova, and J. Van Den Brink, *Nat. Commun.* **8**, 686 (2017).
- [34] A. Hampel, C. Piefke, and F. Lechermann, *Phys. Rev. B* **92**, 085141 (2015).
- [35] Y. K. Kim, O. Krupin, J. D. Denlinger, A. Bostwick, E. Rotenberg, Q. Zhao, J. F. Mitchell, J. W. Allen, and B. J. Kim, *Science* **345**, 187 (2014).
- [36] Y. Cao, Q. Wang, J. A. Waugh, T. J. Reber, H. Li, X. Zhou, S. Parham, S. R. Park, N. C. Plumb, E. Rotenberg, A. Bostwick, J. D. Denlinger, T. Qi, M. A. Hermele, G. Cao, and D. S. Dessau, *Nat. Commun.* **7**, 11367 (2016).
- [37] Y. K. Kim, N. H. Sung, J. D. Denlinger, and B. J. Kim, *Nat. Phys.* **12**, 37 (2015).
- [38] S. Schuwalow, C. Piefke, and F. Lechermann, *Phys. Rev. B* **85**, 205132 (2012).
- [39] J. Chakraborty, S. Samanta, B. R. K. Nanda, and I. Dasgupta, *J. Phys.: Condens. Matter* **28**, 375501 (2016); J. Chakraborty, *ibid.* **29**, 395801 (2017).

*Correction:* The last term in Eq. (3) contained an error and has been fixed.